CONF-8708129--1

THE CHARGE STATE OF IRON IMPLANTED INTO SAPPHIRE

C. J. MCHARGUE, P. S. SKLAD, C. W. WHITE
Oak Ridge National Laboratory, P.O. Box X, Oak Ridge, TN 37831 USA

G. C. FARLOW
Wright State University, Dayton, OH 45435 USA

A. Perez, N. Kornilios, G. Marest
Universite Claude Bernard Lyon I, Villeurbanne Cedex, France

CONF-8708129--1

DE87 014053

ABSTRACT

Single crystals of α-Al_2O_3 were implanted with $^{57}Fe^+$ at room temperature to fluences ranging from 10^{16} to 10^{17} ions/cm^2. The damage in the implanted zone and the valence states and local environment of implanted ions were studied by transmission electron microscopy, Rutherford backscattering-channelling, and conversion electron Mössbauer spectroscopy. The implanted iron was distributed among the three charge states Fe^{2+}, Fe^{3+}, and Fe^0 (metallic clusters) with the relative amount of each varying with concentration (fluence) of implanted iron.

1. INTRODUCTION

The use of ion implantation to modify the near-surface mechanical properties of ceramics is currently being explored at a number of laboratories.[1-3] The changes in hardness, apparent fracture toughness, and flexure strength have been qualitatively related to the damage microstructures. However, the variation in mechanical properties with concentration of implanted ion or between similar concentrations of different chemical species has not been accomplished because detailed information of the local defect structures has not been available.

The nature of defects present in implanted insulating materials (ceramics) will depend upon the residual charge state of the implanted species. In most studies to date, the implanted species has been a cation, therefore, there must be compensation for an excess positive charge.

The use of conversion electron Mössbauer spectroscopy (CEMS) has given insight into the local surroundings of iron implanted into MgO, LiF, and TiO_2 (ref. 4-6). Iron in as-implanted MgO and LiF was present in three well-defined charge states, Fe^{3+}, Fe^{2+}, and Fe^0 (metallic). By studying the variation in the relative amounts of these charge states, these investigators were able to develop models for the defect structures.

2. EXPERIMENTAL CONDITIONS

High-purity Al_2O_3 single crystals having <0001> normal to the surface were given an optical grade polish and then annealed 120 h at 1450°C in flowing oxygen to remove any residual polishing damage. Following this treatment the crystals were almost defect free, as determined by Rutherford backscattering-channeling (RBS) measurements. The minimum yields, χ_m (defined as the ratio of the backscattered yield from a c-axis aligned crystal to that of a random specimen), were 2% in the aluminum sublattice and 8% in the oxygen sublattice.

Crystals were implanted at room temperature using a mass analyzed beam of ^{57}Fe (160 or 100 keV). The fluences covered the range of 10^{16} to 10^{17} ions/cm^2 to give peak iron concentrations of 3 to 30% of cations. The crystals were implanted with the ion beam ~7° off-normal to minimize

channeling effects. Subsequently, the specimens were analyzed by RBS using 2 MeV He^+ ions.

Specimens for transmission electron microscopy (TEM) were prepared in both cross-section and plan view by mechanical polishing followed by ion milling.

Mössbauer spectra were obtained using the technique of conversion electron Mössbauer spectroscopy (CEMS).[7] Two important features of CEMS for studies of implanted materials are: (1) CEMS probes the surface only to a depth of 150 to 200 nm, a thickness comparable to the width of the implanted zone; and (2) Al and O produce low photoelectron backgrounds in conversion-electron detection, thus yielding a high signal to noise ratio.

In the present study, CEMS spectra were determined at 4 K, 77 K, and room temperature using backscattered geometry. The ^{57}Co source was contained in a rhodium matrix and was mounted on a constant acceleration triangular-motion velocity transducer. The data were folded to produce a constant background. The velocity scale and all data are referred to a metallic α-iron absorber. The spectra were fit with a computer least-squares procedure with the assumption of Lorentzian shapes of Mössbauer lines.

3. RESULTS

Micrographs obtained by TEM show the as-implanted microstructure to consist of tangled arrays of dislocations extending from the surface to a depth of about 170 nm. The corresponding electron diffraction patterns showed that the implanted zones remained crystalline. No evidence for precipitates was found, however, the large residual stresses and dense dislocation arrays would prevent the detection of very small precipitate particles as well as the determination of the nature of the dislocations.

The RBS spectra show the residual disorder in the aluminum and oxygen sublattices. The value of χ_{min} at the position of maximum disorder in the Al-sublattice varied from 0.55 (1×10^{16} Fe/cm^2) to 0.82 (1×10^{17} Fe/cm^2), Figs. 1 and 2. Note that Fig. 2 shows the effect of the large concentration of iron (~30 cation %) on the RBS spectra of Al. The fraction of substitutional iron (as viewed along the c-axis) was: 0.86 at 1×10^{16} Fe/cm^2; 0.72 at 2×10^{16} Fe/cm^2; 0.50 at 4×10^{16} Fe/cm^2; and ~ 0 at 1×10^{17} Fe/cm^2. The significance of this measurement in the presence of the disorder at the higher fluences is of course questionable. Nevertheless, the values at the lower fluences may aid in developing a model for the defect structure.

The CEMS spectra measured at room temperature are given in Fig. 3. The spectra consist of the superposition of several overlapping components. The following components were identified on the basis of consistent sets of computer fits for all the spectra: three quadrupole split doublets and one single line. These components can be assigned to a ferric ion (Fe^{3+}), two forms of a ferrous ion (Fe^{2+}_I and Fe^{2+}_{II}) and metallic iron (Fe^0). The Mössbauer parameters (isomershift, IS); quadrupole splitting, QS; linewidths, W; and relative line areas, R, are given in Table 1, and the fluence-dependence of the relative amount of each component is given in Fig. 4.

The ferrous iron, Fe^{2+}, ions are described by two different quadrupole-split doublets characterized by the isomer shifts IS ≈0.7 and 1.15 mm·s^{-1} and the quadrupole splittings QS ≈1.84 and 1.7 mm·s^{-1} for Fe^{2+}_I and Fe^{2+}_{II}, respectively. The parameters for the Fe^{2+}_I component are similar to those for the Fe-O bond in wustite.[8] The Fe^{2+}_{II} component represents a more ionic state and is similar to iron in $FeAl_2O_4$ (ref. 9). Since $FeAl_2O_4$ has partly inverse spinel structure, the iron likely resides in octahedral

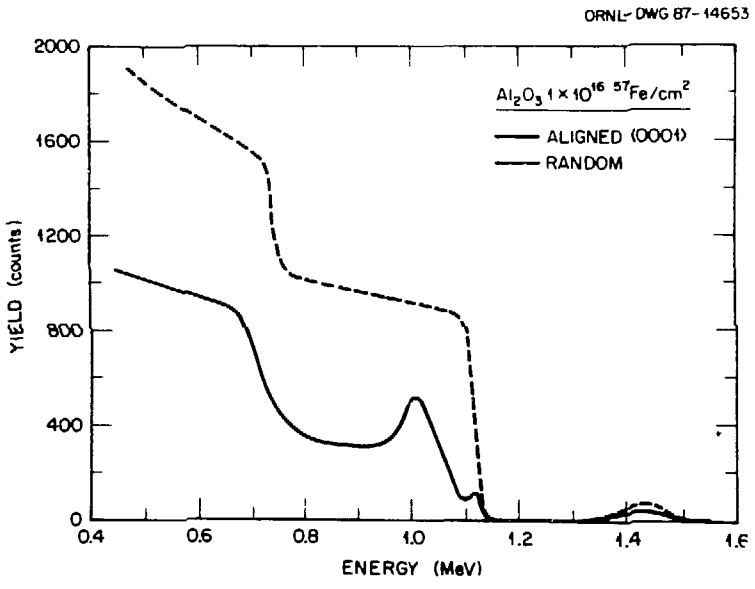

FIGURE 1. Rutherford-backscattering spectra for 2 MeV He^+ from α-Al_2O_3 implanted with 1 × 10^{16} $^{57}Fe/cm^2$ (160 keV) at room temperature.

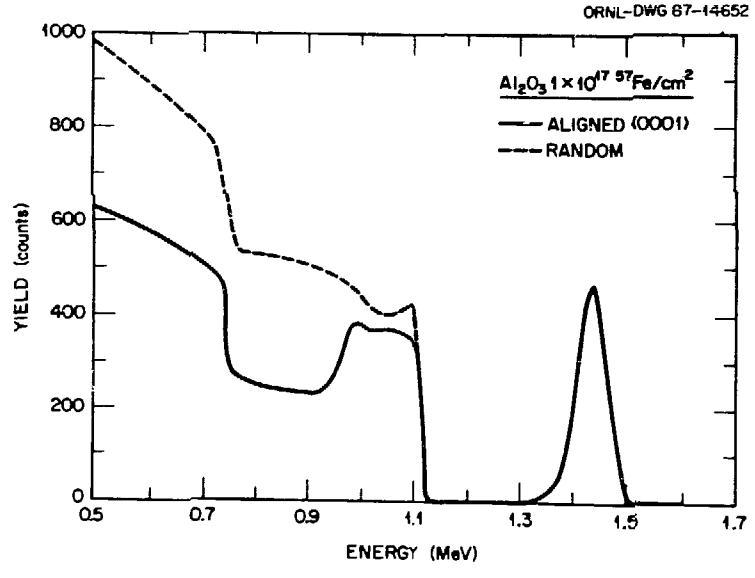

FIGURE 2. Rutherford-backscattering spectra for 2 MeV He^+ from α-Al_2O_3 implanted with 1 × 10^{17} $^{57}Fe/cm^2$ (160 keV) at room temperature.

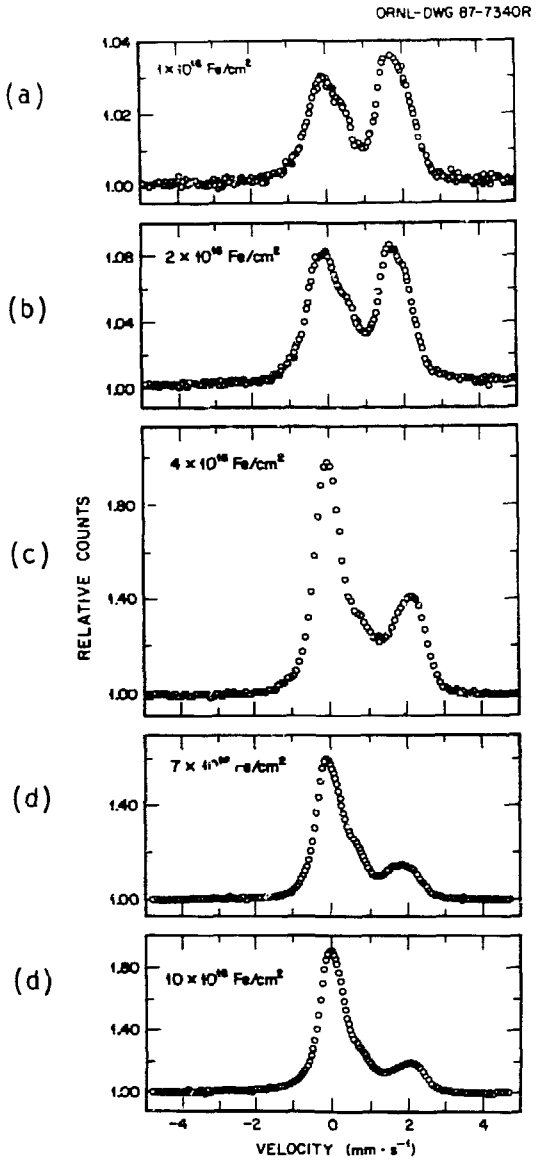

FIGURE 3. Conversion electron Mössbauer spectra measured at room temperature on α-Al_2O_3 implanted with ^{57}Fe: (a) 1×10^{16} ions·cm^{-2} (160 keV), (b) 2×10^{16} ions·cm^{-2} (160 keV), (c) 4×10^{16} ions·cm^{-2} (100 keV), (d) 7×10^{16} ions·cm^{-2} (160 keV), (e) 1×10^{17} ions·cm^{-2} (160 keV).

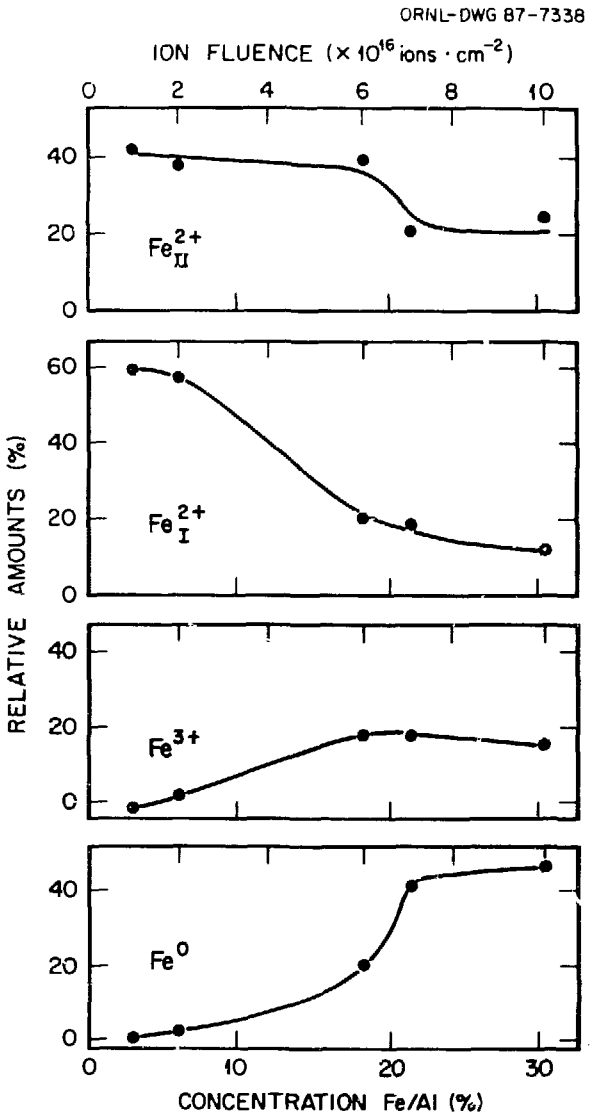

FIGURE 4. Fluence concentration dependence of relative amounts of components present in Mössbauer spectra of iron-implanted Al_2O_3

TABLE 1. Mössbauer parameters of components present in as-implanted Al_2O_3

Fluence (ions cm^{-2})		1×10^{16}	2×10^{16}	4×10^{16}	7×10^{16}	1×10^{17}
E (keV)		160	160	100	160	160
Concentration (Fe:Al)		0.03	0.06	0.18	0.21	0.30
Doublet Fe^{2+}_I	IS ($mm \cdot s^{-1}$)	0.70	0.68	0.69	0.66	0.67
	QS ($mm \cdot s^{-1}$)	1.80	1.86	1.94	1.96	1.85
	W ($mm \cdot s^{-1}$)	0.63	0.65	0.54	0.50	0.55
	R (%)	59	58	21	19	12
Doublet Fe^{2+}_{II}	IS	1.19	1.20	1.14	1.17	1.17
	QS	1.68	1.64	1.94	1.78	1.85
	W	0.66	0.65	0.62	0.55	0.61
	R	41	38	39	20	24
Doublet Fe^{3+}	IS	--	0.24	0.26	0.18	0.22
	QS	--	1.00	1.08	0.97	1.02
	W	--	0.50	0.55	0.38	0.40
	R	--	4	19	18	16
Single Line Fe^0	IS	--	--	-0.09	-0.07	-0.08
	W	--	--	0.48	0.61	0.57
	R	--	--	21	43	48

IS = Isomer Shift
QS = Quadrupole Splitting
W = Line Width
R = Relative Area

sites, consistent with the relatively large value of IS observed. Essentially all the iron resides in the ferrous states at the lower concentrations (fluences) of iron and the relative amount decreases as the implantation fluence increases (Fig. 4), although the total amount in these states continues to increase (Fig. 5).

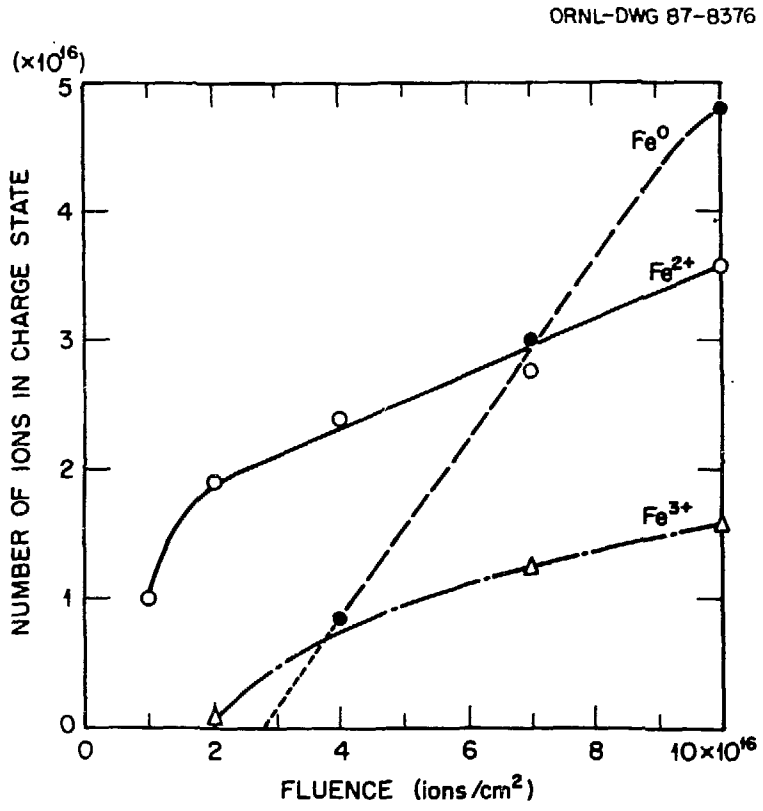

FIGURE 5. Total amounts of each charge state of iron as functions of fluence.

The ferric iron, Fe^{3+}, is represented by a doublet having the parameters: IS ≈0.22 mm·s^{-1}, QS ≈1.0 mm·s^{-1}. These values are comparable to those of iron substitutionally located in alumina $(Al_{1-x}\ Fe_x)_2O_3$ (ref. 10) or amorphous Fe_2O_3 (ref. 11) and are indicative of covalent-distorted octahedral surroundings. the relative amount of this Fe^{3+} component increases from about zero at 1×10^{16} Fe/cm^2 to a maximum of 20% for the high fluence implants.

The single line with IS ≈0 mm·s^{-1} is attributed to small metallic iron precipitates which behave superparamagnetically. The spectra taken at 77 K were similar to the room temperature spectra (Fig. 3e) but those taken at 4 K show magnetic splitting. Figure 6 shows the 4 K spectra after Fourier transform filtering and indicates a superparamagnetic sextet and the Fe^{2+} doublet which distorts the symmetry of the line shapes. Thus, this component arises from small metallic clusters or precipitates with a size of ≈2 nm. The relative fraction of this component increases with fluence and represents about 48% of the implanted iron at the highest fluence.

In the earlier CEMS studies on iron implanted into nonmetallic crystals, attempts were made to use a simple statistical model to analyze the fluence

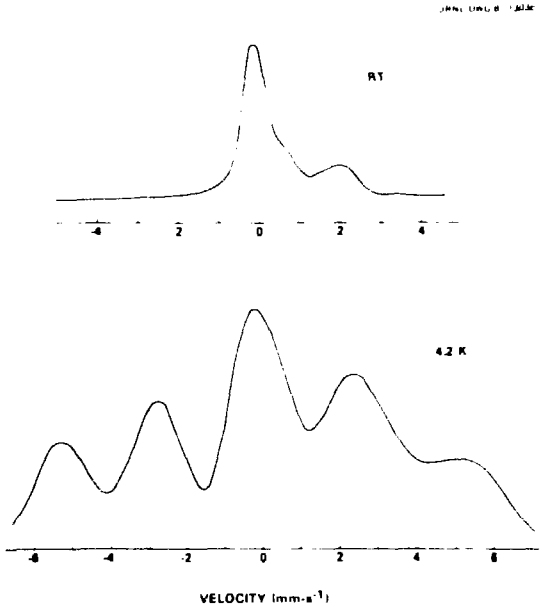

FIGURE 6. Mössbauer spectra obtained at 4 K of specimen implanted with 1×10^{17} Fe/cm^2 (160 keV).

dependence of the charge state.[4,6] The model indicated the trend of the data for LiF and showed quite good fit in the case of MgO. A similar approach was applied to the present data.

The occupancy of the various charge states as functions of fluence was compared with the probability of finding various numbers of iron ions in 1, 2, 3, 4 ... cation coordination shells as a function of iron concentration. This probability was calculated by the binomial distribution:

$$P_N(n,\bar{x}) = \begin{bmatrix} N \\ n \end{bmatrix} \bar{x}^n (1 - \bar{x})^{N-n} ,$$

where N corresponds to the number of neighboring atoms which can be substituted by iron and which form complexes of n impurity atoms with the iron probe atom. Thus, the probability for finding an isolated iron ion (n = 0), two irons (n = 1), etc., can be calculated as a function of iron concentration for 1, 2 ... coordination shells.

The best fit to the experimental findings occurred when four coordination shells were used. Figure 7 shows the fits for the total relative amounts of Fe^{2+}, Fe^{3+}, and Fe^0. The solid line for Fe^{2+} represents the probability of finding a total of 1, 2, or 3 iron atoms within the volume consisting of four cation coordination shells. The curve for Fe^{3+} is the calculated probability of finding exactly four iron atoms within this volume, and that for F^0 represents the probability of finding five or more such atoms. The points are the observed values, taken from Fig. 4. The agreement between these calculations and the data is excellent at low to moderate fluences and less good at the highest fluence where the amount of damage in the Al-sublattice probably makes the concept of near-neighbors questionable.

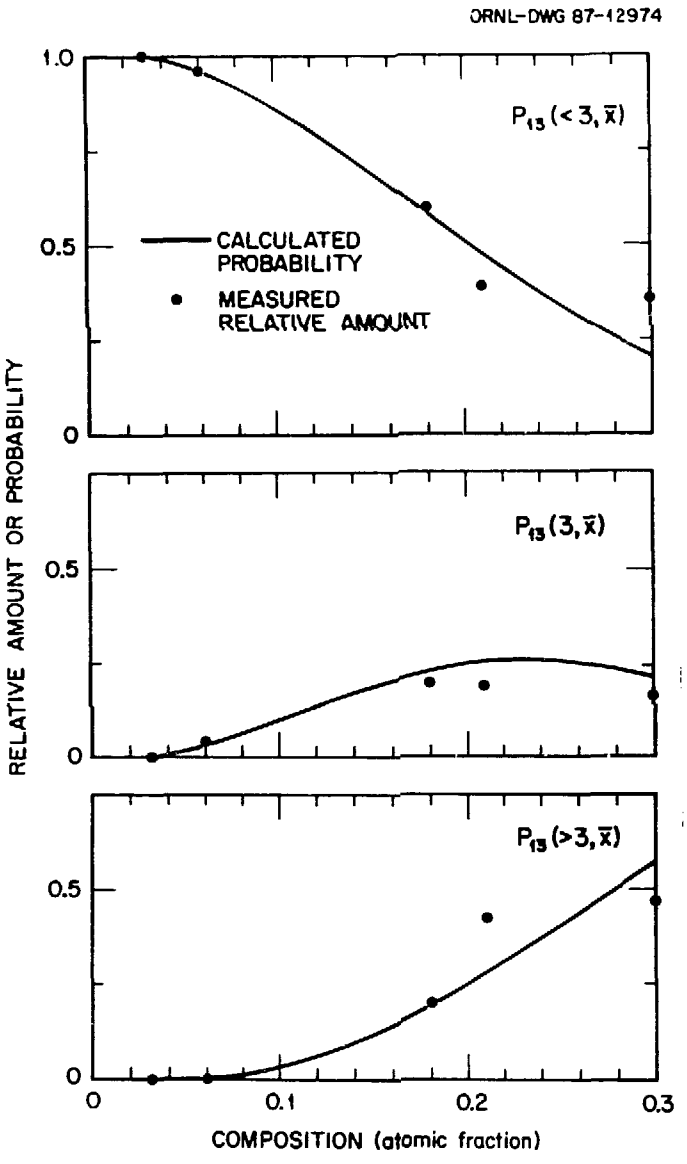

FIGURE 7. Probability for various iron atom configurations in Al_2O_3 lattice calculated from the binomial function. Points are observed relative amounts of Fe^{2+}, Fe^{3+}, and Fe^0.

4. DISCUSSION OF RESULTS

The distribution of the charge states of iron implanted into Al_2O_3 differs significantly from those observed for LiF, MgO, and TiO_2.[4-6] The high fluence implants in those cases resulted primarily in the Fe^{2+} state, with up to 20% of the Fe^0 state in the case of MgO.

The probability calculations suggest that the Fe^{2+} state is occupied when there are 1, 2, or 3 iron ions with four coordination shells. The single iron corresponds to a single interstitial impurity ion and the excess positive charge may be compensated by near-by oxygen interstitials produced by the elastic collisions of the bombarding ions.

The calculated defect energies of Catlow et al.[12] indicate that clustering of defects will dominate upon the introduction of di-valent impurities into Al_2O_3 in the absence of oxygen exchange with the atmosphere. That analysis shows that vacancy compensation in which two impurity ions occupy nearest neighbor sites with respect to an anion vacancy and self-compensation in which the charge on a 2^+ interstitial is

neutralized by two 2^+ impurity ions on substitutional sites located above and below the interstitial along the c-axis. The calculations indicate the vacancy mode to be preferred.

The vacancy compensation mode has the configuration $Fe^{2+}_S - \square_O - Fe^{2+}_S$ or two neighboring iron ions, while the self-compensating configuration is $Fe^{2+}_S - Fe^{2+}_i - Fe^{2+}_S$, or three neighboring iron ions. A consistent scheme for the defect structure involving the ferrous ions is:

One Fe^{2+} in four coordination shells = isolated interstitial

Two Fe^{2+} in four coordination shells = two Fe^{2+} substitutionals plus one oxygen vacancy

Three Fe^{2+} in four coordination shells = two Fe^{2+} substitutionals plus one Fe^{2+} interstitial

The ferric state, Fe^{3+}, appears to be a direct substitution of Fe^{3+} for Al^{3+}, either in the Al-sublattice or within the stoichiometric interstitial loop damage structure proposed by Pells and Stathopoulos.[13] It is not yet clear as to why this configuration is preferred for exactly four iron ions within the four coordination shells.

At high fluences (concentrations) of iron, the probability of forming clusters dominates and the large excess positive charge is avoided by formation of the metallic iron clusters. There is ample opportunity for the iron ions to capture electrons since much of the incident energy is lost by inelastic (electronic) processes.

The Mössbauer line associated with the small metallic iron clusters (or precipitates) has an isomer shift of about -0.08 mm·s^{-1} relative to bulk α-iron (bcc). There are two possible reasons for obtaining such a value rather than IS ≈ 0. The isomer shift for γ-iron (fcc) is also -0.08 mm·s^{-1}, suggesting that the initial configuration of the very small particle could be face-centered cubic. Annealing studies (to be reported elsewhere) shows that the value of IS goes to zero as the particles increase in size during annealing. A second possibility is that the clusters are initially under very high isostatic pressures which increases the electron density at the nucleus and thus decreases the isomer shift.

5. SUMMARY

Several techniques (RBS, TEM, CEMS) have been used to characterize sapphire single crystals implanted with iron at room temperature to fluences of 10^{16} to 10^{17} ions cm^{-2}. At low fluences the as-implanted iron is found mainly in the ferrous state. As the fluence is increased, Fe^{3+} and metallic iron clusters become dominant. There is a strong correlation between the probability of finding specific configurations of iron ions within four cation coordination shells and the relative amount of each charge state observed. The superparamagnetic behavior of the clusters suggest that they are of the order of 2 nm in size but the large amount of irradiation-induced damage and residual stress has prevented their imaging by TEM.

Research sponsored in part by the Division of Materials Sciences, U.S. Department of Energy, under contract DE-AC05-84OR21400 with the Martin Marietta Energy Systems, Inc.

REFERENCES

1. McHargue CJ: Nucl. Instrum. Methods Phys. Res. B19/20, 797 (1987).
2. Barnett PJ and Page TF: J. Mater. Sci. 19, 3524 (1984).
3. Hioki T, Itoh A, Noda S, Doi H, Kawamoto J, and Kamigaito O: J. Mater. Sci. Lett. 3, 1099 (1984).
4. Perez A, Marest G, Sawicka BD, Sawicki JA, and Tyliszczak T: Phys. Rev. B 28, 1227 (1983).
5. Kowalski J, Marest G, Perez A, Sawicka BD, Sawicki JA, Stanek J, and Tyliszczak T: Nucl. Instrum. Methods 209/210, 1145 (1983).
6. Guermazi M, Marest G, Perez A, Sawicka BD, Sawicki JA, Thevenard P, and Tyliszczak T: Mat. Res. Bull. 18, 529 (1983).
7. Sawicka BD and Sawicki JA: pp. 139–66 in Topics in Current Physics, Vol. 25, ed. U. Gonser, Springer, Berlin 1981.
8. Greenwood NN and Gibb TC: pp. 249 in Mössbauer Spectroscopy, Chapmann and Hall Ltd., London, 1971.
9. Rossiter MJ: J. Phys. Chem. Solids 26, 775 (1965).
10. Janet C and Gilbert H: Bull. Soc. Fr. Mineral. Cristallogr. 93, 213 (1970).
11. Van Diepen AM and Popma Th. JA: Solid State Commun. 27, 121 (1978).
12. Catlow CRA, James R, Mackrodt WC, and Stewart RF: Phys. Rev. B 25, 1006 (1982).
13. Pells GP and Stathopoulos AY: Rad. Eff. 74, 181 (1983).